Available online at www.sciencedirect.com
SCIENCE DIRECT®
Applied Catalysis A: General 255 (2003) 45–57
APPLIED CATALYSIS A: GENERAL
www.elsevier.com/locate/apcata

Perovskites as catalysts precursors: CO_2 reforming of CH_4 on $Ln_{1-x}Ca_xRu_{0.8}Ni_{0.2}O_3$ (Ln = La, Sm, Nd)

M.R. Goldwasser [a,*], M.E. Rivas [a], E. Pietri [a], M.J. Pérez-Zurita [a], M.L. Cubeiro [a], L. Gingembre [b], L. Leclercq [b], G. Leclercq [b]

[a] *Centro de Catálisis, Petróleo y Petroquímica, Escuela de Química, Facultad de Ciencias, Universidad Central de Venezuela, Apartado 47102, Los Chaguaramos, Caracas, Venezuela*
[b] *Université des Sciences ET Technologies de Lille, Laboratoire de Catalyse Hétérogene ET Homogène, 59655 Villeneuve Dásc, Cedex, France*

Received 29 August 2002; received in revised form 19 December 2002; accepted 19 December 2002

Abstract

A series of perovskite-like oxide in which the A-site cation of the precursor perovskite, $LaRu_{0.8}Ni_{0.2}O_3$, was partially or totally substituted by calcium, samarium and neodymium have been used to produce in situ nanoparticles of Ru(Ni) well dispersed on a stable support for the carbon dioxide reforming of methane. Perovskites of the type $Ln_xCa_{1-x}Ru_{0.8}Ni_{0.2}O_3$ ($Ln = La^{3+}, Sm^{3+}, Nd^{3+}$) were synthesized as catalysts precursors. The reduced solids of nominal composition (Ru,Ni)/CaO and/or La_2O_3, Sm_2O_3, Nd_2O_3, were used as catalysts.

The $La_{1-x}Ca_xRu_{0.8}Ni_{0.2}O_3$ series showed a well-defined perovskite structure with surface areas between 3 and 10 m^2/g. However, when lanthanum was replaced by samarium and neodymium, the presence of pyrochlore structures, together with the perovskites, were obtained. After reduction Ru(Ni) crystallites size between 9 and 17 nm were produced. The substitution of La by cations of smaller ionic radii (Ca, Nd, Sm) decrease the stability of the perovskites and lower their reduction temperature. Among the calcium series, $La_{0.8}Ca_{0.2}Ru_{0.8}Ni_{0.2}O_3$ and $La_{0.5}Ca_{0.5}Ru_{0.8}Ni_{0.2}O_3$, proved to be the most active catalysts with the highest selectivity to CO. While samarium-containing perovskite was the best among the lanthanide series.

Correlations between the effect of partial or total substitution of A-site cations of the precursor perovskite and the catalytic activity and stability of in situ formed nickel and ruthenium particles were established.

Keywords: CO_2 reforming of methane; Ru–Ni perovskites; Syngas production; Calcium promotion; Effect of lanthanides

1. Introduction

The need to preserve the environment has prompted the international community to dictate a series of regulations that affect, decrease or increase the price of the activities of the petroleum industry; introducing legal statutes that have to be accomplished by conventional fuels in the short term. In this context, the carbon dioxide reforming of methane emerges as an alternative especially for global environmental protection, since both reactants are thought to contribute to global warming. In addition, this process allows the production of syngas with a H_2/CO ratio more convenient for further applications: while higher H_2/CO ratio favors methane and inhibit chain growth [1–3], a low H_2/CO ratio favors the methanol to gasoline process for ethane, propane and aromatics from methanol

* Corresponding author. Fax: +58-212-239-21-62.
E-mail address: mgoldwas@reacciun.ve (M.R. Goldwasser).

0926-860X/$ – see front matter © 2003 Published by Elsevier B.V.
doi:10.1016/S0926-860X(03)00643-4

[4]. Alkenes, oxygenates, hydroformylation and acetic acid production are also favored at low H_2/CO ratios [5–8].

However, the drawback of carbon dioxide reforming of methane is deactivation of catalysts caused by carbon deposition. This serious problem could be inhibited by the use of highly dispersed metal species according to the concept of ensemble size control [9–13]. The use of precursors, such as perovskite-like oxides ABO_3, in which A-site cation is a rare earth and/or alkaline earth and B-site cation is a transition metal, could be the answer to these problems. Perovskites not only fulfill the stability requirements, but also by further reduction of B-site cations which remain distributed in the structure, they result in the formation of a well-dispersed and stable metal particle catalyst [14–16]. Previous studies on $CaRuO_3$ [17], $LaCoO_3$ [18] and $LaNiO_3$ [19] perovskites indicate that by reduction treatment, the metal (Ru, Co, Ni) is in a highly disperse state on a matrix composed of the respective metal oxide. Similarly, it has been established that the right combination of metal support strongly affect not only the coke formation but also the activity of reforming catalysts, as shown by Zhang and Verykios [20] and Eldöhelyi et al. [21] for Rh and Pd, respectively, over different supports.

Although many previous investigations of the CO_2 reforming of methane have been carried out over transition metals supported on alumina, silica and magnesia [9,13,20,22–26], the use of perovskite-type oxides has been less studied [14–16,27].

Recently, we have reported [15,16] that the best combination for Ru–Ni when working with $LaRu_{1-x}Ni_xO_3$ as precursor perovskites was $LaRu_{0.8}Ni_{0.2}O_3$. Since the properties of the precursor perovskite could be changed depending on the choice and stoichiometry of A- and B-site cations, we decided to study the effect of such changes. Following these ideas, we use calcium as A-site cation due to its basic character, which should further inhibit coke formation. Calcium is a well-known promoter of steam reforming catalysts, its influence on particle size distribution has been previously reported. Goula et al. [28] and Tang et al. [13] over Ni/Al_2O_3 catalysts reported that the presence of CaO influenced the morphology and particle size distribution of nickel metal, inhibiting coke deposition. Similarly, Choudary et al. [23] reported the enhancement of activity of Ni catalysts when the support (Al_2O_3 or SiO_2) was precoated with CaO.

The aim of this paper is to stabilize small particles of Ru–Ni over a stable support (Ca, Ln oxides) to prevent carbon formation in the carbon dioxide reforming of methane. The effect of substitution of lanthanum by other lanthanides, such as samarium and neodymium, was also studied. Perovskites of the type $Ln_xCa_{1-x}Ru_{0.8}Ni_{0.2}O_3$ (Ln = La^{3+}, Sm^{3+}, Nd^{3+}) were synthesized as catalysts precursors. The reduced solids of nominal composition (Ru,Ni)/CaO and/or La_2O_3, Sm_2O_3, Nd_2O_3, were used as catalysts to establish correlations between the effect of partial or total substitution of A-site cations of the precursor perovskite and the catalytic activity and stability of in situ formed nickel and ruthenium particles.

2. Experimental

2.1. Synthesis and characterization of the precursor perovskites

The perovskite-type oxides $Ln_{1-x}Ca_xRu_{0.8}Ni_{0.2}O_3$ (Ln = La, Sm, Nd) were synthesized by a modification of the citrate method [29]. Adequate amounts of the precursor of B-site cations ($RuCl_3{\cdot}xH_2O$ and $Ni(NO_3)_2{\cdot}6H_2O$), were dissolved in citric acid (99.5 Riedel-de Haën) with an excess of ethylene glycol (99.5 Riedel-de Haën) as the organic polydentate ligand. $La(NO_3)_3{\cdot}6H_2O$, $Ca(NO_3)_2{\cdot}4H_2O$, $Sm(NO_3)_3{\cdot}6H_2O$, $Nd(NO_3)_3{\cdot}6H_2O$ were used as A-site cations precursors.

The solids were characterized before and after catalytic tests by means of different techniques. Inductively Coupled Plasma Emission Spectroscopy (ICP) using a Perkin-Elmer ICP/5500 instrument analyzed the chemical compositions (Ru, Ni, La, Ca, Sm, and Nd) of the perovskite products. The IR spectra of the final product were recorded in a Perkin-Elmer 283 spectrometer between 1200 and 400 cm^{-1}. BET surface areas were determined by nitrogen–argon adsorption at 77 K with an N_2/Ar ratio of 30/70 using a Micromeritics model ASAP 2010. X-ray diffraction (XRD) experiments were conducted using a Siemens D-8 advanced diffractometer with a Cu Kα radiation for crystalline phase detection between 20 and 90° (2θ) and under temperature-programmed reduction (TPR)

in H_2. JCPDS-ICDD standard spectra software was used to determine the phases. The ruthenium crystallite size was calculated using Ru(1 0 1) reflection and the Scherrer formula [26,30] with Warren's correction for instrumental line broadening $dv = 0.9\lambda/[(\beta^2 - B^2)^{1/2}\cos\theta]$, where $\lambda = 1.54056$ Å and the line broadening at 44° 2θ is $B = 0.09°$, by means of TOPAS P Profile Fitting Program from Brucker Analytical X-ray System. TPR was carried out in a Thermo-Quest TPD/TPR 1100 system using 0.07 g of the sample in an 8% H_2/92% Ar stream (20 cm^3/min). For the TPR analysis, the temperature was raised from room temperature to 120 °C at a rate of 10 °C/min, then holding it for 15 min to remove any adsorbed water, and raised it again up to 900 °C for 2 h. The X-ray Photoelectron Spectroscopy (XPS) analyses were performed with a VG ESCALAB 220 XL spectrometer. The monochromatized Al Kα (1486.6 eV) source was operated at 80 W. The residual vacuum at the analysis chamber was always better than 5×10^{-8} Torr. All the solids were studied before and after reduction. For the XPS analysis, the reduction treatments were conducted in situ using H_2 as reducing agent and left 9 h at 500 °C (heating rate 2 °C/min). Auto-coherent references were used: La3$d_{5/2}$ at 833.8 eV, Ru3$d_{5/2}$ at 280.2 eV and O1s at 529.3 eV.

2.2. Catalytic tests

Activity tests were performed using 200 mg of catalyst in a 20 mm i.d. quartz reactor at atmospheric pressure operated in a fixed-bed continuous flow system ($CH_4/CO_2 = 1$, N_2 as diluents, 723–1123 K, a total flow of 80 ml/min and WHSV = 24 l/h g.). Before the catalytic tests, the solids were reduced in H_2 flow (20 ml/min, $T = 700$ °C, 8 h). After reduction, the system was swept with N_2 for 15 min and adjusted to reaction temperature. The water produced during reaction was condensed before passing the reactants and products to the analyzing system, which consisted of an on-line gas chromatograph (Perkin-Elmer Auto System XL) equipped with a TCD and provided with a Carbosieve SII 80/100 (12′ × 1/8″ o.d. SS). The conversions of CH_4 and CO_2 were defined as the converted CH_4 and CO_2 per total amount of CH_4 and CO_2 feeded, respectively. The selectivity for product "*i*" was defined as $\%S_i = N_i/(N\mathrm{CH_4}\,(c) + N\mathrm{CO_2}\,(c)) \times 100$, where $N\mathrm{CH_4}$ (c) and $N\mathrm{CO_2}$ (c) are the amount of converted methane and carbon dioxide. Coke deposition on the catalysts after reaction was determined by elemental analysis using a LECO C-144 Carbon Determination, with a detection limit of 50 ppm and a precision ≤1%.

3. Results and discussion

Results will be discussed considering two series of catalysts, one in which the lanthanum perovskite $LaRu_{0.8}Ni_{0.2}O_3$ is modified by calcium, named Ca–La series, and the other in which $La_{0.8}Ca_{0.2}Ru_{0.8}Ni_{0.2}O_3$ is modified by samarium and neodymium, named the lanthanide series.

3.1. Perovskites characterization: surface area, chemical analysis, IR and XRD

Table 1 lists the synthesized perovskite and the ICP analysis. A close similarity between analytical and nominal values in each case was observed. However, an oxygen deficiency was shown by all synthesized perovskites.

In order to assess the presence of the perovskite-like structures, XRD and IR spectra were recorded. The IR spectra for all the solids showed two broad bands characteristics of ABO_3 perovskites centered around 400 and 600 cm^{-1}. Their positions are in good agreement with those reported in the literature [15,16,31]. Surface area, IR bands, cell parameters and corresponding symmetry are shown in Table 2.

Most of the synthesized solids showed areas higher than 3 m^2/g, a decrease in surface area was observed as Ca substituted La, with the lowest value shown by the higher calcium-containing perovskites (3 m^2/g). It is interesting to note that within the Ca–La series, those precursor perovskites with the higher surface areas showed the best catalytic activity ($La_{0.8}Ca_{0.2}Ru_{0.8}Ni_{0.2}O_3$ and $La_{0.5}Ca_{0.5}Ru_{0.8}Ni_{0.2}O_3$). When calcium was substituted by the lanthanides, an increase in surface area was observed for lanthanum and samarium perovskites (from 3 to 9 m^2/g) while no change was observed for the neodymium perovskite.

For the Ca–La series, the XRD patterns of the as synthesized solids at room temperature revealed that the perovskite structure was the main phase detected, although some deviations from the perfect

Table 1
Chemical analysis

Perovskites	Ln (%)		Ca (%)		Ru (%)		Ni (%)		O (%)	
	Nominal values	Analytical values	Nominal values	Analytical values	Nominal values	Analytical values	Nominal values	Analytical values	Nominal values	Analytical values
$LaRu_{0.8}Ni_{0.2}O_3$	49.70	45.30	–	–	28.93	20.75	4.20	4.43	17.17	16.12
$La_{0.8}Ca_{0.2}Ru_{0.8}Ni_{0.2}O_3$	42.78	42.91	3.09	3.16	31.13	28.08	4.52	4.56	18.48	18.23
$La_{0.5}Ca_{0.5}Ru_{0.8}Ni_{0.2}O_3$	30.19	29.62	8.71	8.46	35.14	32.73	5.10	5.04	20.86	16.66
$La_{0.2}Ca_{0.8}Ru_{0.8}Ni_{0.2}O_3$	13.86	13.57	16.00	14.69	40.35	39.49	5.86	5.49	23.95	19.62
$CaRu_{0.8}Ni_{0.2}O_3$	–	–	22.18	17.83	44.75	44.96	6.50	6.35	26.57	23.53
$Sm_{1.8}Ca_{0.2}RuNiO_{5.8}$ $Sm_2Ru_2O_7$	44.74	41.98	2.98	1.96	30.07	29.13	4.36	4.23	17.80	15.79
$Nd_{1.8}Ca_{0.2}RuNiO_{5.8}$ $Nd_2Ru_2O_7$	43.71	41.98	3.04	2.27	30.63	27.54	4.45	4.30	18.18	17.24

stoichiometry resulted in small quantities of other phases. All perovskites could be indexed with an orthorhombic or cubic symmetry of the ABO_3 type with the exception of $Sm_{0.8}Ca_{0.2}Ru_{0.8}Ni_{0.2}O_3$ and $Nd_{0.8}Ca_{0.2}Ru_{0.8}Ni_{0.2}O_3$ that showed a perovskite structure mixed with a pyrochlore. On these solids, the perovskite-type structures correspond to double perovskites, such as Ln_2RuNiO_6 (JCPDS-ICDD file 45-0658), in which part of the lanthanide cation has been replaced by calcium. The pyrochlore structure formed between samarium and ruthenium (JCPDS-ICDD file 28-0997) and between neodymium and ruthenium (JCPDS-ICDD file 28-0673) could be due to the difference of ionic radii between samarium and neodymium with respect to that of calcium, since both lanthanides have ionic radii smaller than calcium. The variation of the lattice parameters with composition is shown in Table 2.

3.2. Temperature-programmed reduction and in situ XRD

The relative stability of the perovskites in reducing atmosphere was determined, for all solids, by in situ XRD and by TPR. The XRD patterns for $La_{0.8}Ca_{0.2}Ru_{0.8}Ni_{0.2}O_3$ and $La_{0.2}Ca_{0.8}Ru_{0.8}Ni_{0.2}O_3$, as synthesized and reduced at different temperatures, are shown in Figs. 1 and 2, respectively. The room temperature patterns for both perovskites show peaks at 2θ 23, 33, 47, 58 for $La_{0.2}Ca_{0.8}Ru_{0.8}Ni_{0.2}O_3$ and at 32, 46, 56, 66 for $La_{0.8}Ca_{0.2}Ru_{0.8}Ni_{0.2}O_3$ which correspond almost exactly to $CaRuO_3$ perovskite (JCPDS file 82-1476) and $LaRuO_3$ perovskite (JCPDS file 82-1477). It is observed that when the temperature is raised, cations in position B are reduced to metals while those in position A are transformed to the respective oxides. For the Ca–La series, the most drastic

Table 2
Surface area, IR bands, symmetry and cell parameters of synthesized solids

Perovskites	Area (m^2/g)	IR bands		Symmetry[a]	Cell parameters (Å)		
		ν_1	ν_2		*a*	*b*	*c*
$LaRu_{0.8}Ni_{0.2}O_3$	9	592	417	O	5.52	7.88	5.54
$La_{0.8}Ca_{0.2}Ru_{0.8}Ni_{0.2}O_3$	8	600	418	C	7.86	7.86	7.86
$La_{0.5}Ca_{0.5}Ru_{0.8}Ni_{0.2}O_3$	10	568	465	O	5.51	7.79	5.50
$La_{0.2}Ca_{0.8}Ru_{0.8}Ni_{0.2}O_3$	6	–	–	O	5.36	7.67	5.53
$CaRu_{0.8}Ni_{0.2}O_3$	3	–	–	O	5.36	7.66	5.53
$Sm_{1.8}Ca_{0.2}RuNiO_{5.8}$	9	576	431	O	5.67	7.67	5.43
$Sm_2Ru_2O_7$				C	10.59	10.59	10.59
$Nd_{1.8}Ca_{0.2}RuNiO_{5.8}$	2	578	413	O	5.44	7.74	5.67
$Nd_2Ru_2O_7$				C	10.61	10.61	10.61

[a] Symmetry: O = orthorhombic, C = cubic.

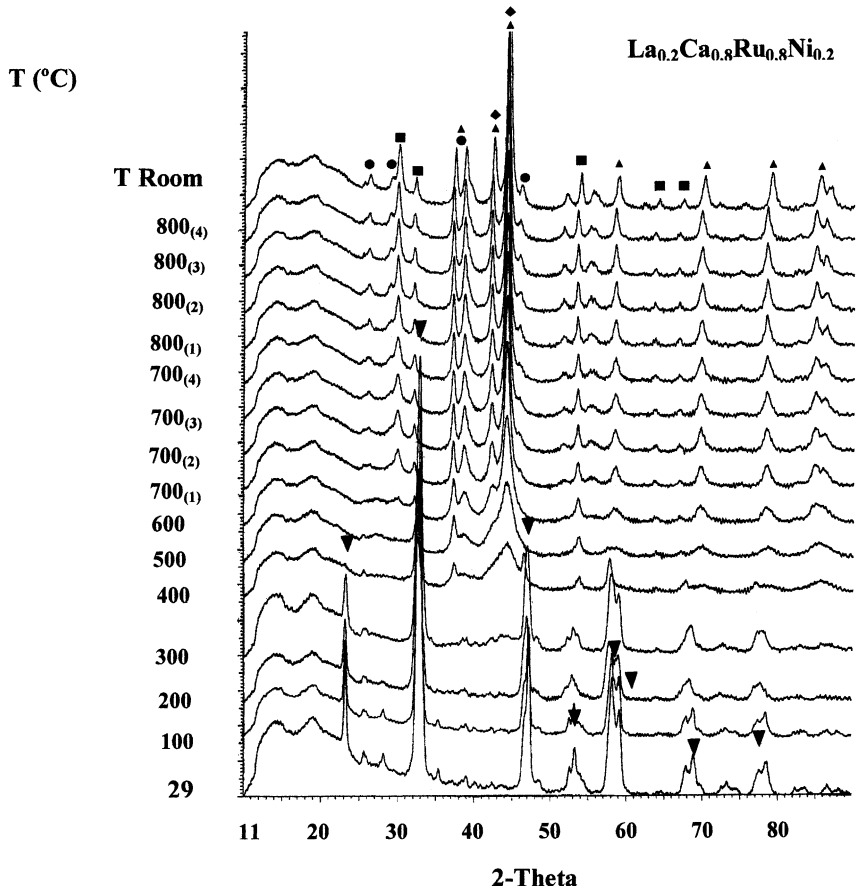

Fig. 1. In situ XRD of $La_{0.2}Ca_{0.8}Ru_{0.8}Ni_{0.2}O_3$ as synthesized and reduced at different temperatures. (#) Time in hours at a given temperature; (◆) Ni; (●) La_2O_3; (▲) Ru; (■) CaO; (▼) perovskite.

changes are seen between 300 and 400 °C for the higher calcium content perovskites (Fig. 1, Table 3), while for the more lanthanum-containing samples, degradation of the perovskite start at 400–500 °C (Fig. 2, Table 3). The perovskite is progressively degraded until approximately 700 °C. Perovskites with a higher lanthanum content being more stables. For all solids, the observed phases after reduction at

Table 3
In situ XRD results: phases and average size of Ru(Ni) after reduction

Samples	Degree[a] (2θ)	T of degradation (°C)	Phases after reduction	Mean size (nm)
$LaRu_{0.8}Ni_{0.2}O_3$	32.100	400–500	Ru^0, Ni^0, La_2O_3	9.9
$La_{0.8}Ca_{0.2}Ru_{0.8}Ni_{0.2}O_3$	32.230	400–500	Ru^0, Ni^0, CaO, La_2O_3	10.3
$La_{0.5}Ca_{0.5}Ru_{0.8}Ni_{0.2}O_3$	32.486	300–500	Ru^0, Ni^0, CaO, La_2O_3	15.1
$La_{0.2}Ca_{0.8}Ru_{0.8}Ni_{0.2}O_3$	32.887	300–400	Ru^0, Ni^0, CaO, La_2O_3	17.4
$CaRu_{0.8}Ni_{0.2}O_3$	32.912	300–400	Ru^0, Ni^0, CaO	14.9
$Ca_{0.2}Sm_{0.8}Ru_{0.8}Ni_{0.2}O_3$	32.700	400–600	Ru^0, Ni^0, CaO, Sm_2O_3	10.7
$Ca_{0.2}Nd_{0.8}Ru_{0.8}Ni_{0.2}O_3$	32.480	400–600	Ru^0, Ni^0, CaO, Nd_2O_3	9.2

[a] Evolution of the most intense peak at 29 °C.

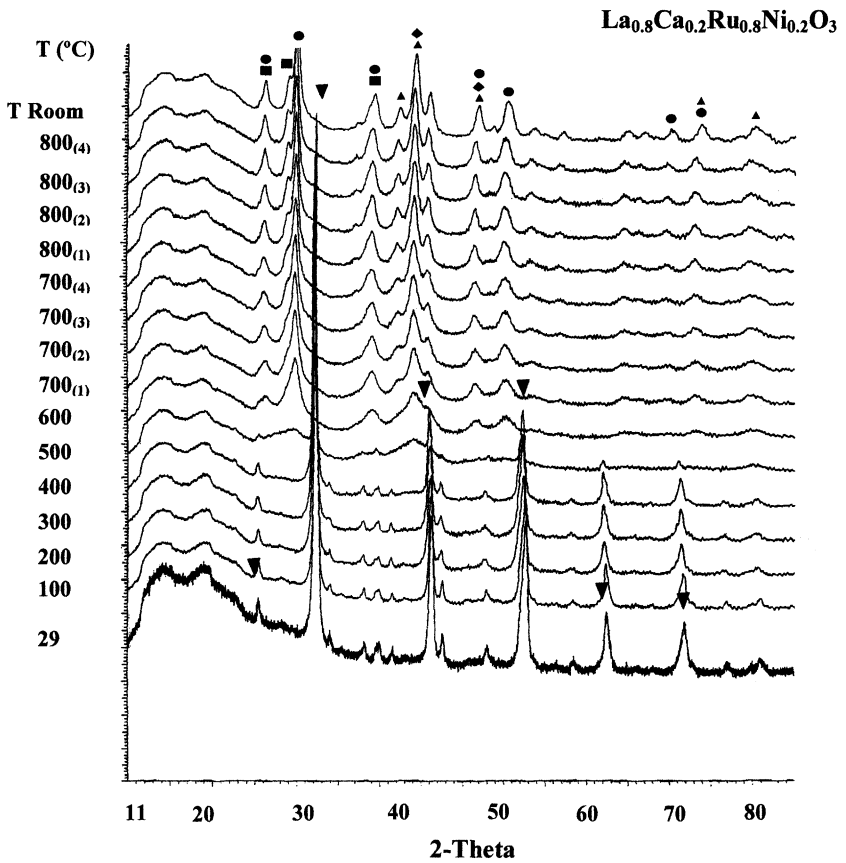

Fig. 2. In situ XRD of $La_{0.8}Ca_{0.2}Ru_{0.8}Ni_{0.2}O_3$ as synthesized and reduced at different temperatures. (#) Time in hours at a given temperature; (◆) Ni; (●) La_2O_3; (▲) Ru; (■) CaO; (▼) perovskite.

800 °C were: Ru metal (alone or alloyed with Ni), CaO and La_2O_3 in different proportions depending on the composition of the starting perovskite.

A similar behavior was shown by TPR (Fig. 3). The temperature, at which an increase in hydrogen consumption is observed, coincided with that where changes were seen by XRD for these solids. The TPR indicate that, in general, the perovskite reduction proceeds in two steps. A first peak, with a maximum at around 200–400 °C depending on the perovskite, and a second peak appearing above 400 °C. Hurst et al. [33] suggest for ruthenium and nickel on different supports that the first peak is due to the reduction of the Ru^{3+} to Ru^{2+} and/or Ni^{3+} to Ni^{2+}, while the second peak at higher temperature is due to the reduction of the Ru^{2+} and/or Ni^{2+} to Ru^0 and Ni^0. In our case, the XRD in situ reduction results seems to indicate that the first peak of reduction could be attributed to weakly bound Ru–Ni cations and to residues of the precursors. This could be inferred from the fact that for all studied perovskites the diffraction peaks remain essentially in the same position up to 350 °C (Figs. 1 and 2, Table 2) changing only in intensity. The second peak could be attributed to a simultaneously Ru and Ni reduction to produce Ru^0 and Ni^0 probably with an alloy formation. Even that formation of an alloy could not be verified, the position of the peaks at 2θ 44.2, intermediate to that of 44.00 for hexagonal Ru (JCPDS file 06-0663) and 44.505 for cubic Ni (JCPDS file 04-0850) are in favor of this possibility.

When lanthanum is partially substituted by calcium, a shift to lower temperatures is clearly observed (Fig. 3). The substitution of an A-site cation by another of lower valence could significantly influence

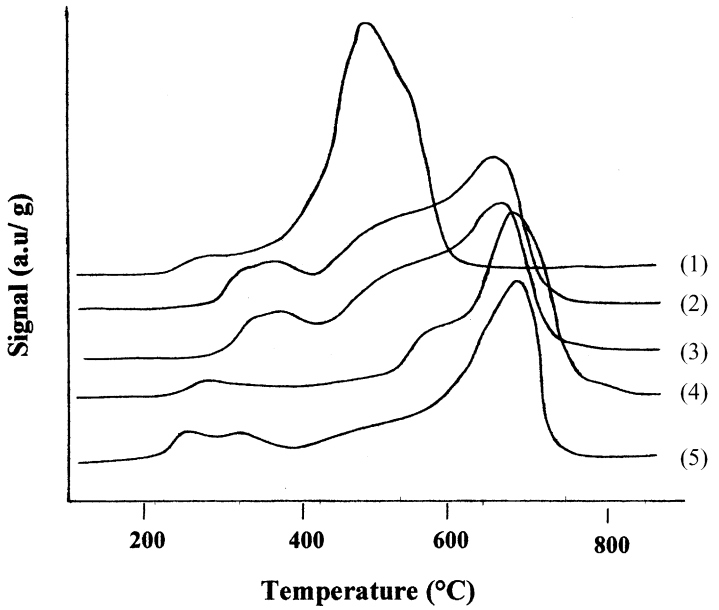

Fig. 3. TPR profiles of Ca–La series: (1) $CaRu_{0.8}Ni_{0.2}O_3$; (2) $La_{0.2}Ca_{0.8}Ru_{0.8}Ni_{0.2}O_3$; (3) $La_{0.5}Ca_{0.5}Ru_{0.8}Ni_{0.2}O_3$; (4) $La_{0.8}Ca_{0.2}Ru_{0.8}Ni_{0.2}O_3$; (5) $LaRu_{0.8}Ni_{0.2}O_3$.

the reducibility of the perovskite [32,34–37]. This effect is attributed to the fact that a cation of lower ionic radium (Ca^{2+}) is replacing one of higher radium (La^{3+}), which decreases the stability of the perovskite structure, increasing the mobility of the oxygen in the structure and facilitating its elimination as water during reduction. In order for the structure to remain stable after the substitution of La^{3+} by Ca^{2+}, charge compensation is needed. This could be achieved through the existence of some Ru and/or Ni ions with valence states higher than 3+, or by formation of an oxygen-deficient perovskite of the type $ABO_{3-\lambda}$. The ICP and XPS results indicate that the second statement is taking place since a deficiency of oxygen was observed for these solids. These changes in the precursor perovskites favor their reducibility as seen by the reduction pattern of the perovskites: the higher the calcium contents the easier the reduction of the perovskites. The observed ease of reduction was: $CaRu_{0.8}Ni_{0.2}O_3 > La_{0.2}Ca_{0.8}Ru_{0.8}Ni_{0.2}O_3 > La_{0.5}Ca_{0.5}Ru_{0.8}Ni_{0.2}O_3 > La_{0.8}Ca_{0.2}Ru_{0.8}Ni_{0.2}O_3 > LaRu_{0.8}Ni_{0.2}O_3$. As expected, lanthanum the largest ion in the series forms the most stable perovskite structure [14,37].

For the lanthanide series, an additional effect was observed (Fig. 4). Samarium- and neodymium-containing perovskites showed two very intense peaks, while for lanthanum perovskite a sharp peak was observed at high temperature, with a small peak at low temperature. This is in agreement with the XRD results for the neodymium and samarium solids, where a mixture of perovskites and pyrochlore phases was observed. The presence of these mixed phases, make structures less stable, which reflects in a higher reduction facility compared to lanthanum perovskite.

XRD analysis was also used to determine the metal particles size of the crystallites by means of the Scherrer equation [26,30]. Sizes were calculated at around 44° (2θ), which correspond to the most intense band for Ru metal (44.37°), very close to that of Ni (44.50°). With the exception of the catalyst from $LaRu_{0.8}Ni_{0.2}O_3$, on the perovskites reduced at 800 °C, peaks correspond mainly to Ru, slightly shifted in comparison to Ru alone, due to the presence of Ni. For $LaRu_{0.8}Ni_{0.2}O_3$ the intensity of the Ru–Ni peak is wider indicating that the crystallites does not change with temperature, while for the more calcium-containing perovskites the destruction starts

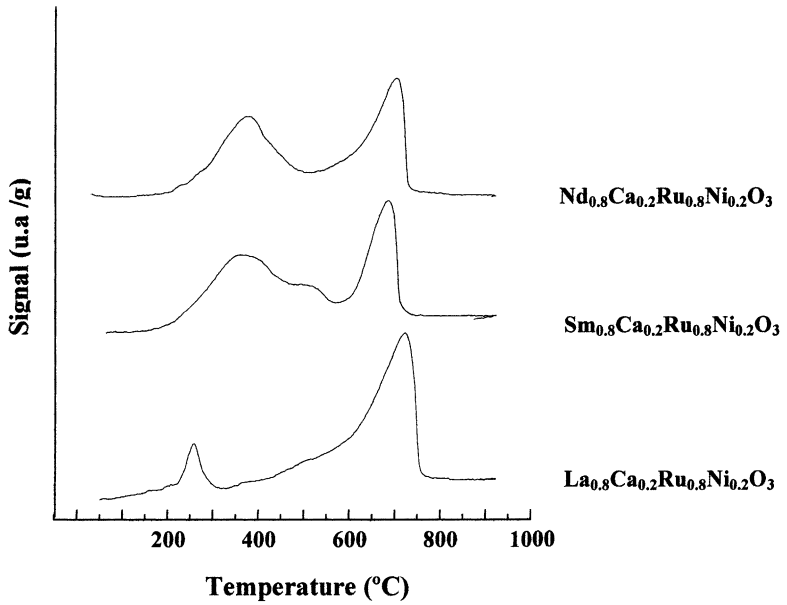

Fig. 4. TPR profiles of lanthanide series.

when the temperature start raising (300 °C) and the metal peaks become sharper indicating the presence of larger particles. Lanthanum seems to stabilize the Ru(Ni) metal crystallites. In addition, an inverse relationship seems to exist between the size of the metallic crystallites and the temperature at which the second reduction peak appears in the TPR. The higher the temperature of the second peak, the smaller the particle size. It appears as if during the destruction of the perovskite by reduction, the metallic ions are being released in a controlled way avoiding formation of large metallic clusters by sinterization. For all structures, the mean particle size values are between 9 and 17 nm (Table 3), indicating a high dispersion and/or uniform distribution of Ru(Ni) in the $CaO–Ln_2O_3$ matrix after reduction. These values are smaller than those reported by Choudary et al. [19] for Ni^0/La_2O_3 obtained from $LaNiO_3$ (31.3 nm) and much smaller than that (125 nm) for $NiO–La_2O_3$ [38]. These results corroborate the advantage of the sol–gel method to obtain metallic supported nanoparticles [13,15,16,25].

After reaction, the identified phases were Ru^0, Ni^0, CaO, $CaCO_3$ and Ln_2O_3. The carbonate observed on these solids is formed from reaction of the oxides by decomposition of the precursor perovskite and CO_2 from the reaction mixture. Those perovskites with a high lanthanum content ($LaRu_{0.8}Ni_{0.2}O_3$ and $La_{0.8}Ca_{0.2}Ru_{0.8}Ni_{0.2}O_3$) also show peaks corresponding to lanthanum dioxomonocarbonate, $La_2O_2CO_3$. This phase, which is in fast equilibrium with the carbon dioxide in the gas phase during reaction, has been claimed as responsible for the no-deactivation of the catalyst by carbon [15,16,20,22,32].

3.3. X-ray Photoelectron Spectroscopy

The XPS results of both Ca–La and lanthanide series showed that under the experimental conditions used only B cations (Ru and Ni) are reduced to the zero oxidation state, while those cations in position A do not show any reduction.

For Ca–La series it was observed that the presence of calcium leaves the La 3d doublets very much unaffected, except for a very small displacement (0.2 eV) towards lower binding energies. For the lanthanide series, the presence of lanthanum, samarium or neodymium did not affect the binding energy of the Ca 2p signals. Again, as for the Ca–La series only metals in position B were completely reduced.

To evaluate the chemical state and evolution of the metals at the surface, a semi-quantitative analysis was performed. Only Ru/O and Ru/(A + A′) ratios are

Table 4
Bulk and surface stoichiometry of the reduced perovskites

Samples		La	Ca	Ru	Ni	O	Ru/O	Ru/(Ca + La)	[Ru/O]/[Ru/(Ca + La)]
$LaRu_{0.8}Ni_{0.2}O_3$	Surface	1.0	–	0.15	0.08	1.34	0.11	0.15	0.73
	Bulk	1.0	–	0.80	0.20	3.00	0.27	0.80	0.34
$La_{0.8}Ca_{0.2}Ru_{0.8}Ni_{0.2}O_3$	Surface	1.0	0.42	0.35	–	1.55	0.23	0.25	0.92
	Bulk	0.8	0.20	0.80	0.20	3.00	0.27	0.80	0.34
$La_{0.5}Ca_{0.5}Ru_{0.8}Ni_{0.2}O_3$	Surface	1.0	0.55	0.68	–	1.53	0.44	0.44	1.00
	Bulk	0.5	0.50	0.80	020	3.00	0.27	0.80	0.34
$La_{0.2}Ca_{0.8}Ru_{0.8}Ni_{0.2}O_3$	Surface	1.0	0.38	0.28	–	1.45	0.19	0.20	0.95
	Bulk	0.2	0.80	0.80	0.20	3.00	0.27	0.80	0.34
$CaRu_{0.8}Ni_{0.2}O_3$	Surface	0.0	1.00	0.22	0.17	0.94	0.23	0.22	0.96
	Bulk	0.0	1.00	0.80	0.20	3.00	0.27	0.80	0.34
$Ca_{0.2}Sm_{0.8}Ru_{0.8}Ni_{0.2}O_3$	Surface	0.5[a]	0.33	0.40	0.10	1.00	0.40	0.47	0.85
	Bulk	0.8[a]	0.20	0.80	0.20	3.00	0.27	0.80	0.34
$Ca_{0.2}Nd_{0.8}Ru_{0.8}Ni_{0.2}O_3$	Surface	0.8[a]	1.00	0.32	0.17	2.06	0.16	0.18	0.89
	Bulk	0.8[a]	0.20	0.80	0.20	3.00	0.27	0.80	0.34

[a] Sm or Nd.

presented since attempts to extract reliable quantification of Ni was extremely difficult due to the severe covering of the Ni 2p signals by the complex La 3d region. This situation was worsened by the low nickel content of the perovskites. Similarly, quantification of neodymium in the presence of lanthanum is difficult: Nd 4d is perturbed by La 4d, and the most intense signal Nd 3d interfere with the Auger peaks of oxygen (Al source). Table 4 shows a comparison of the stoichiometry of the bulk and surface of reduced perovskites.

If it is assumed that for the Ca–La series Ru^0, CaO and La_2O_3 are the main phases present after reduction, as observed by XRD, the Ru/O ratio should be around three times smaller than that of Ru/La [39,40]. However, it is observed that the substitution of lanthanum by calcium lead to a Ru/O ratio approximately equal to that of Ru/La indicating a great deficiency in oxygen. These results are in good agreement with ICP and TPR observations, where the formation of an oxygen-deficient perovskite of the type $La_{1-x}Ca_xRu_{0.8}Ni_{0.2}O_{3-\lambda}$ was invoked to compensate for the difference in charge produced when Ca^{2+} substitutes La^{3+}. In agreement with TPR and XRD results, the observed oxygen deficiency was lower for the most stable perovskite $LaRu_{0.8}Ni_{0.2}O_3$.

3.4. Catalytic studies

In previous work [15,16], the effect of parameters, such as reaction temperature, space velocity, reactant partial pressure and time on stream, was investigated and optimized to higher yields of syngas. It was found that the best Ru–Ni combination was obtained for $LaRu_{0.8}Ni_{0.2}O_3$. In the present work, partial or total substitution of lanthanum by calcium was carried out, to increase the basicity of the catalysts in order to inhibit coke formation.

The study was started with $La_{0.5}Ca_{0.5}Ru_{0.8}Ni_{0.2}0_3$ perovskite under previous optimized conditions. For this solid, it was observed that the previously used reduction conditions were not sufficient to reach total transformation of B-site cations. Under these conditions (T_R = 700 °C, $T_{Red.}$ = 700 °C/3 h), the obtained catalyst showed a lower activity compared to that of the reference perovskite $LaRu_{0.8}Ni_{0.2}0_3$. Consequently, both reaction temperature and reduction time were increased to 800 °C and 8 h, respectively. Under these conditions, the catalyst from $La_{0.5}Ca_{0.5}Ru_{0.8}Ni_{0.2}0_3$ showed a higher activity. Methane and CO_2 conversions were 98 and 77%, respectively, with a CO selectivity of 86% (Table 5).

The next step was to study the effect of calcium content on the precursor perovskite. The following

Table 5
Catalytic activity

Samples	800 °C			700 °C		
	XCH_4 (%)	XCO_2 (%)	SCO (%)	XCH_4 (%)	XCO_2 (%)	H_2/CO (%)
$LaRu_{0.8}Ni_{0.2}O_3$	78.6	83.9	85.4	89.2	66.6	0.81
$La_{0.5}Ca_{0.5}Ru_{0.8}Ni_{0.2}O_3$	98.85	76.7	85.8	49.2	41.3	–
$La_{0.8}Ca_{0.2}Ru_{0.8}Ni_{0.2}O_3$	99.77	76.6	90.3	84.9	61.7	0.86
$La_{0.2}Ca_{0.8}Ru_{0.8}Ni_{0.2}O_3$	99.30	83.2	73.6	45.9	50.2	–
$CaRu_{0.8}Ni_{0.2}O_3$	99.8	88.9	76.9	55.9	48.9	–
$Nd_{1.8}Ca_{0.2}RuNiO_{5.8}$ $Nd_2Ru_2O_7$	96.35	78.3	81.8	84.8	60.3	0.82
$Sm_{1.8}Ca_{0.2}RuNiO_{5.8}$ $Sm_2Ru_2O_7$	95.47	84.8	81.1	85.7	68.6	0.84
Commercial catalyst	99.77	85.3	75.6	94.28	70.72	0.90

$T_R = 800$, 700 °C, $t_{reac} = 24$ h, WHSV = 24 l/h g, $CH_4/CO_2 = 1$, $(PCH_4 + PCO_2)/P_T = 0.2$, $W = 200$ mg, $T_{Red.} = 700$ °C/8 h.

perovskites were prepared: $La_{0.8}Ca_{0.2}Ru_{0.8}Ni_{0.2}O_3$, $La_{0.2}Ca_{0.8}Ru_{0.8}Ni_{0.2}O_3$ and $CaRu_{0.8}Ni_{0.2}O_3$. It was observed that as the content of calcium increases in the perovskite (Fig. 5), a decrease in the induction period (time needed for the precursor perovskite to start showing activity) was decreased as compared to the reference perovskite $LaRu_{0.8}Ni_{0.2}O_3$, in agreement with the TPR and in situ XRD experiments where reduction was easier for those perovskites. Their catalytic activity is shown in Table 5. As observed, at 800 °C most catalysts showed CH_4 conversions near 100%, with the best selectivity to CO (90%) achieved by $La_{0.8}Ca_{0.2}Ru_{0.8}Ni_{0.2}O_3$.

To maintain conversions away from thermodynamic equilibrium, the temperature was adjusted to 700 °C. Fig. 6 shows the influence of calcium content on these perovskites. A decrease in conversion as lanthanum is substituted by calcium was observed, being higher for CH_4 than for CO_2. However, the selectivity to CO remains almost constant. Among this series, the best activity was obtained for $La_{0.8}Ca_{0.2}Ru_{0.8}Ni_{0.2}O_3$. The fact that CO_2 conversion was always lower than that of methane and that H_2/CO ratios lower than 1, indicates the occurrence of other reactions. Partial combustion of methane by oxygen present in the nitrogen (∼2%) used as diluent could not be discarded.

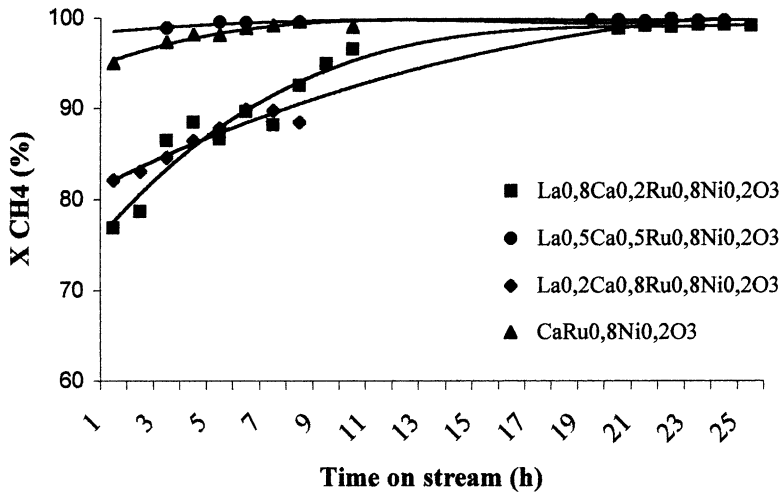

Fig. 5. Methane conversion vs. time on stream for Ca–La series. $T_R = 800$ °C, WHSV = 24 l/h g, $CH_4/CO_2 = 1$, $(PCH_4 + PCO_2)/P_T = 0.2$, $W = 200$ mg, Red. = 700 °C/8 h.

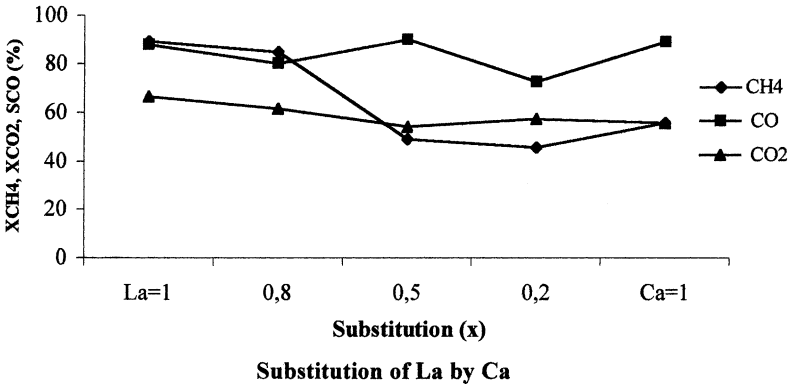

Fig. 6. Effect of substitution of La by Ca vs. time on stream. $T_R = 700\,^{\circ}C$, WHSV = 24 l/h g, $CH_4/CO_2 = 1$, $(PCH_4 + PCO_2)/P_T = 0.2$, $W = 200$ mg, Red. = 700 °C/8 h.

Since $La_{0.8}Ca_{0.2}Ru_{0.8}Ni_{0.2}O_3$ showed the best catalytic activity for both sets of experimental conditions, as observed from Table 5, the next step was to study the influence of the substitution of lanthanum by other lanthanides, such as samarium and neodymium. The initial tests were carried out at 800 °C maintaining other variables constant. As observed in Table 5, the methane and CO_2 conversion and the selectivity to CO were very high. Even at 700 °C an increase in CO selectivity for samarium- and neodymium-containing perovskite and a small increase in methane and CO_2 conversion was observed compared to that shown by lanthanum perovskite (Fig. 7).

Under the optimized experimental conditions, catalysts did not show significant coke deposition even after 120 h on stream (1.38% carbon/g of catalyst), maintaining their activity and selectivity to CO (Fig. 8), which corroborate the low coke formed in these solids. When working with supported nickel catalyst for steam reforming, Trimm [10] suggested that the presence of rare earth oxides added to the support should diminish coke formation by favoring coke gasification. This could be the case since on $La_{0.8}Sm_{0.2}Ru_{0.8}Ni_{0.2}O_3$ only 0.51% of carbon/g of catalyst was observed [41].

Comparison with an industrial catalyst containing 12% Ni, used for steam reforming of methane, was

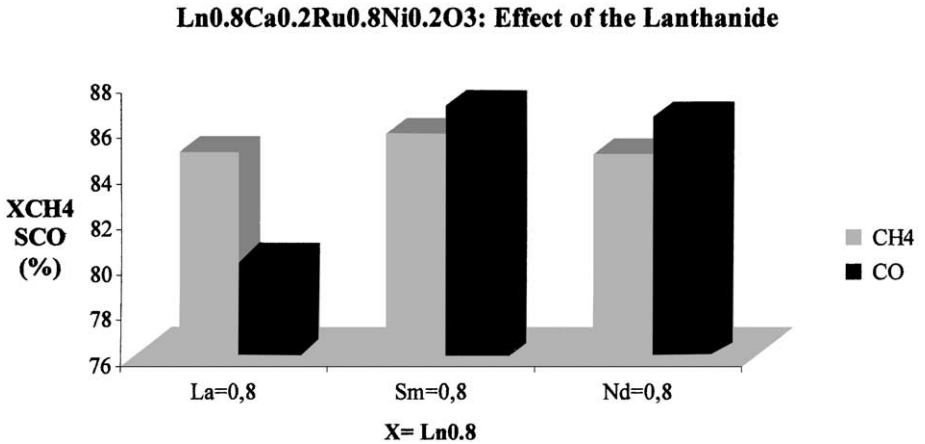

Fig. 7. $Ln_{0.8}Ca_{0.2}Ru_{0.8}Ni_{0.2}O_3$: effect of lanthanides. $T_R = 700\,^{\circ}C$, WHSV = 24 l/h g, $CH_4/CO_2 = 1$, $(PCH_4 + PCO_2)/P_T = 0.2$, $W = 200$ mg, Red. = 700 °C/8 h.

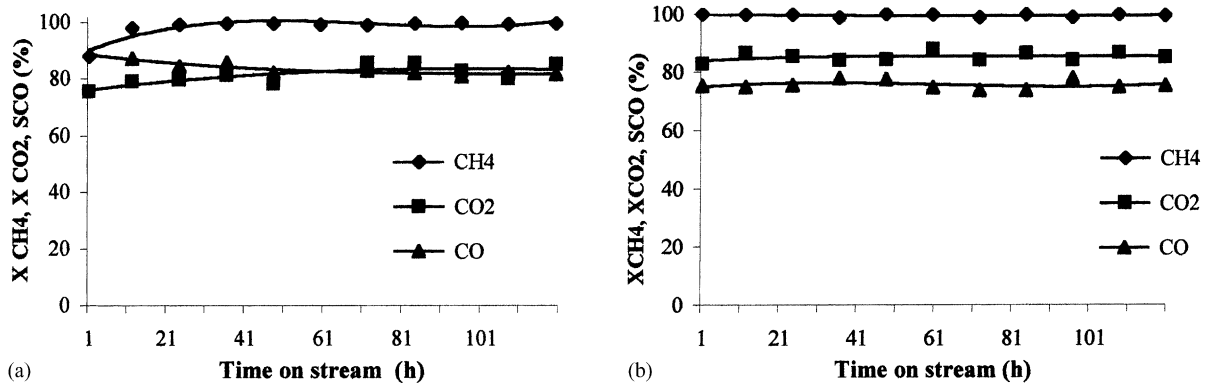

Fig. 8. Stability test: (a) $Ln_{0.5}Ca_{0.5}Ru_{0.8}Ni_{0.2}O_3$; (b) commercial catalyst. $T_R = 800\,^{\circ}C$, WHSV = 24 l/h g, $CH_4/CO_2 = 1$, $(PCH_4 + PCO_2)/P_T = 0.2$, $W = 200$ mg, Red. = 700 °C/8 h.

carried out. The conversions of methane, CO_2, and the selectivity to CO and the stability of the commercial catalyst were similar to that shown by catalysts obtained from the perovskites precursors (Fig. 8, Table 5), which evidence that further improvement of catalysts prepared by using the perovskites looks promising.

4. Conclusions

Preparation of the precursor perovskites by the sol–gel method produces solids with a high homogeneity and crystallinity as confirmed by the different characterization techniques. The Ca–La series $La_{1-x}Ca_xRu_{0.8}Ni_{0.2}O_3$ showed a well-defined perovskite structure. However, when lanthanum is replaced by samarium and neodymium, the presence of pyrochlore structures, together with the perovskites, were observed as evidenced by the XRD analysis.

The TPR curves of the precursor perovskites showed that the substitution of lanthanum by cations of smaller ionic radii (Ca, Nd, and Sm) favored the reactivity of the lattice oxygen, which gives rise to lower stability of the perovskite and lower temperature of reduction.

Reduction before reaction of the precursor perovskites produced small Ru–Ni nanoparticles that avoid coke formation and give rise to active and stable catalysts.

When the best reaction conditions were determined ($T_R = 800\,^{\circ}C$, $T_{Red.} = 700\,^{\circ}C/8$ h), all catalysts showed high conversion and good selectivity to CO. Among the Ca–La series, the solids with the best catalytic performance were: $La_{0.8}Ca_{0.2}Ru_{0.8}Ni_{0.2}O_3$ and $La_{0.5}Ca_{0.5}Ru_{0.8}Ni_{0.2}O_3$, with the highest selectivity to CO.

It was observed that the unchanged composition of B-site cations of the precursor perovskites keeps approximately constant the methane and CO_2 conversions, while the change of the nature and composition in A-site cations of the precursor perovskite strongly modifies the stability and selectivity of the catalysts.

Acknowledgements

The authors thank Venezuelan FONACIT for its financial support through Agenda Petroleum Project No. 97-003739.

References

[1] E. Iglesias, Appl. Catal. A: Gen. 161 (1997) 59.
[2] M. BjØrgen, S. Kolboe, Appl. Catal. A: Gen. 225 (2002) 285.
[3] J.R. Rostrup-Nielsen, Stud. Surf. Sci. Catal. 81 (1994) 25.
[4] D. Kitchen, A. Pinto, Ammonia Plant Saf. Relat. Facil. 31 (1991) 219.
[5] M.E. Dry, Catal. Today 71 (2002) 227.
[6] M.L. Cubeiro, H. Morales, M.R. Goldwasser, M.J. Pérez-Zurita, F. González-Jiménez, React. Kinet. Catal. Lett. 69 (2000) 259.

[7] J.R. Rostrup-Nielsen, Catal. Today 71 (2002) 243.
[8] L. Guczi, Zs. Koppány, K.V. Sarma, L. Borkó, I. Kiricsi, Stud. Surf. Sci. Catal. 105 (1997) 861.
[9] K. Tomishige, O. Yamazaki, Y. Chen, K. Yokoyama, X. Li, K. Fujimoto, Catal. Today 45 (1998) 35.
[10] D.L. Trimm, Catal. Today 49 (1999) 3.
[11] J.R. Rostrup-Nielsen, Stud. Surf. Sci. Catal. 68 (1991) 85.
[12] I. Alstrup, N.T. Andersen, J. Catal. 104 (1987) 466.
[13] S. Tang, L. Ji, J. Lin, H.C. Zeng, K.L. Tan, K. Li, J. Catal. 194 (2000) 424.
[14] L.G. Tejuca, J.L.G. Fierro (Eds.), Properties and Applications of Perovskite-type Oxides, New York, 1992, p. 271.
[15] E. Pietri, A. Barrios, M.R. Goldwasser, M.J. Pérez-Zurita, M.L. Cubeiro, J. Goldwasser, L. Leclercq, G. Leclercq, L. Gingembre, Stud. Surf. Sci. Catal. 30 (2000) 3657.
[16] E. Pietri, A. Barrios, O. Gonzalez, M.R. Goldwasser, M.J. Pérez-Zurita, M.L. Cubeiro, J. Goldwasser, L. Leclercq, G. Leclercq, L. Gingembre, Stud. Surf. Sci. Catal. 136 (2001) 381.
[17] A. Reller, G. Davoodabady, A. Portmann, H.R. Oswald, Proceedings of the 8th European Congress on Electron Microscopy, Budapest, 1984.
[18] M. Crespin, W.K. Hall, J. Catal. 69 (1981) 359.
[19] V.R. Choudary, B.S. Uphade, A.A. Belhekar, J. Catal. 163 (1996) 312.
[20] Z.L. Zhang, X.E. Verykios, Appl. Catal. A: Gen. 138 (1996) 109.
[21] A. Eldöhelyi, J. Cserényi, E. Papp, F. Solymosi, Appl. Catal. A: Gen. 108 (1994) 205.
[22] A. Slagtern, Y. Schuurman, C. Leclercq, X. Verykios, C. Mirodatos, J. Catal. 172 (1997) 118.
[23] V.R. Choudary, B.S. Uphade, A.S. Mamman, Catal. Lett. 32 (1995) 387.
[24] V.A. Tsipouriari, X.E. Verykios, Catal. Today 64 (2001) 83.
[25] V.C.H. Kroll, H.M. Swaan, C. Mirodatos, J. Catal. 161 (1996) 409.
[26] M.C.J. Bradford, M.A. Vannice, Appl. Catal. A: Gen. 142 (1996) 73.
[27] Y. Wu, O. Kawaguchi, T. Matsuda, Bull. Chem. Soc. Jpn. 71 (1998) 563.
[28] M.A. Goula, A.A. Lemonidou, A.M. Efstathiou, J. Catal. 161 (1996) 626.
[29] M.P. Pechini, United States Patent Office 3,330,673 (1967).
[30] H.P. Klug, L.E. Alexander, X-ray Diffraction Procedures for Polycrystalline and Amorphous Materials, Wiley, London, 1962, p. 491.
[31] C.P. Khattak, D.E. Cox, Mater. Res. Bull. 12 (1977) 463.
[32] N. Matsui, K. Anzai, N. Akamatsu, K. Nakagawa, N. Okikenaga, T. Suzuki, Appl. Catal. A: Gen. 179 (1999) 247.
[33] N.W. Hurst, S.J. Gentry, A. Jones, B.D. McNicol, Catal. Rev. Sci. Eng. 24 (1982) 233.
[34] W.Y. Hown, R.J. Thorn, J. Phys. Chem. Solids 41 (1980) 75.
[35] M. Stajanović, R.G. Haverkamp, C.A. Mims, H. Mudallal, A.J. Jacobson, J. Catal. 165 (1997) 315.
[36] L.G. Tejuca, J.L.G. Fierro, J.M.D. Tascon, Adv. Catal. 36 (1989) 237.
[37] P. Ciabelli, S. Cimino, S. De Rossi, M. Faticanti, L. Lisi, G. Minelli, I. Pettiti, P. Porta, G. Russo, M. Turco, Appl. Catal. B: Env. 24 (2000) 243.
[38] V.R. Choudary, V.H. Rane, A.M. Rajput, Catal. Lett. 22 (1993) 289.
[39] J.A. Marcos, R.H. Buitriago, E.A. Lombardo, J. Catal. 105 (1987) 95.
[40] H. Falcón, M.J. Martinez-Lope, J.A. Alonso, J.L.G. Fierro, Appl. Catal. B: Env. 26 (2000) 131.
[41] M.R. Goldwasser, et al. (unpublished results).